Surface-Confined Macrocyclization via Dynamic Covalent Chemistry

# Surface-Confined Macrocyclization *via* Dynamic Covalent Chemistry

Chaoying Fu,[1,2,3] Jiří Mikšátko,[4] Lea Assies,[3] Vladimír Vrkoslav,[5] Silvia Orlandi,[6] Martin Kalbáč,[4] Petr Kovaříček,[4] Xiaobin Zeng,[1] Boping Zhou,[1*] Luca Muccioli,[6,7*] Dmitrii F. Perepichka,[3*] Emanuele Orgiu[2*]

[1] *Center Lab of Longhua Branch and Department of Infectious disease, Shenzhen People's Hospital, 2nd Clinical Medical College of Jinan University, Shenzhen 518120, Guangdong Province, China.*

[2] *INRS, Énergie Matériaux Télécommunications Centre, 1650 boulevard Lionel-Boulet, Varennes (Québec) J3X 1S2, Canada*

[3] *Department of Chemistry, McGill University, 801 Sherbrooke Street W., Montreal, QC, Canada H3A 0B8*

[4] *J. Heyrovsky Institute of Physical Chemistry of the Czech Academy of Sciences, Dolejškova 2155/3, 182 23 Praha, Czech Republic*

[5] *Institute of Organic Chemistry and Biochemistry of the Czech Academy of Sciences, Flemingovo náměstí 542/2, 166 10 Praha, Czech Republic*

[6] *Dipartimento di Chimica Industriale "Toso Montanari", Università di Bologna, 40136, Bologna, Italy*

[7] *Institut des Sciences Moléculaires, UMR 5255, University of Bordeaux, 33405 Talence, France*

*Corresponding authors :* zhou.boping@szhospital.com , luca.muccioli@unibo.it , dmitrii.perepichka@mcgill.ca , emanuele.orgiu@emt.inrs.ca

**Abstract**

Surface-confined synthesis is a promising approach to build complex molecular nanostructures including macrocycles. However, despite the recent advances in on-surface macrocyclization under ultra-high vacuum, selective synthesis of monodisperse and multicomponent macrocycles remains a challenge. Here we report on an on-surface formation of [6+6] Schiff-base macrocycles *via* dynamic covalent chemistry. The macrocycles form 2D crystalline domains on the micrometer scale, enabled by dynamic conversion of open chain oligomers into well-defined ~3.0 nm hexagonal macrocycles. We further show that by tailoring the length of the alkyl substituents, it is possible to control which of three possible products -oligomers, macrocycles or polymers- will form at the surface. *In situ* scanning tunneling microscopy imaging combined with density functional theory calculations and molecular dynamics simulations unravel the synergistic effect of surface confinement and solvent in leading to preferential on-surface macrocyclization.

**Keywords**: dynamic covalent chemistry, on-surface synthesis, macrocycle, scanning tunneling microscopy, density functional theory, molecular dynamics simulation

Since the discovery of crown ethers in the mid-1960s,[1] the intriguing structure of macrocycles and their host-guest interactions[2] had tantalized several generation of scientists, and gave birth to an entirely new discipline, supramolecular chemistry.[3] Many macrocycles have found applications in medicinal chemistry,[4,5] catalysis,[6,7] sensing[8,9] and optoelectronics.[10,11] However, chemical synthesis of macrocycles is often challenging and low-yielding, fundamentally limited by the unfavorable entropy of the head-to-tail cyclization of the linear oligomeric intermediates. Solution synthesis of such macrocycles usually requires highly diluted reaction conditions[10,12] to suppress intermolecular propagation reactions, as well as metal-templated preorganization[13,14] to thermodynamically favor intramolecular cyclization *versus* the intermolecular polymerization.

Recently, the on-surface chemistry was shown to provide a promising alternative for synthesis of well-defined macrocyclic molecules.[15] The surface confinement restricts the conformational and rotational freedom of the molecular precursors.[16] Moreover, solid surfaces can function as a template to guide hierarchical coupling of reaction intermediates into atomically precise nanostructures.[17-20] This approach has recently been applied to synthesize oligophenylene,[21-24] oligothiophene,[25,26] heterotriangulene[27,28] and graphdiyne[29] macrocycles *via* Ullmann coupling on transition metal surfaces under ultrahigh vacuum (UHV) conditions. However, since the used reactions (most commonly, Ullmann coupling) are kinetically controlled,[15,19,30] they inevitably introduce structural defects and often lead to polydisperse nanorings of various shapes and sizes.[21-24,26,29] Besides, the UHV conditions required for such surface-catalyzed synthesis limit the versatility of this approach and multicomponent on-surface reactions have been seldom reported.[31]

Dynamic covalent chemistry (DCC) offers a potential solution to both aforementioned issues, by allowing the system to achieve (the pre-programmed) thermodynamic minimum and by enabling the reaction at ambient condition at the solid-liquid interface.[32,33] These features have been well demonstrated in an increasing number of reports on surface-supported synthesis of DCC-linked covalent organic frameworks, that are characterized by a small amount of defects and high surface coverage.[34-38] Hitherto, DCC has not yet been successfully implemented in on-surface synthesis of macrocycles, except for the attempted synthesis of cyclic sexiphenylenes *via* olefin metathesis,[39] and [3+3] macrocycles *via* Schiff-base condensation on graphite surfaces.[40] However, these endeavours resulted in the predominant formation of linear oligomers and only negligible amounts of cyclic compounds, across different reaction conditions (*i.e.* temperature, pressure, concentration, and pH). Interestingly, the authors suggested that surface adsorption and solvent effects significantly alter the product distribution of DCC at the solid-liquid interface. In conclusion, the limited current understanding of the DCC at the solid-liquid interface precludes its use for efficient macrocyclic formation.

Here we make a step forward by reporting the successful [6+6] macrocyclization at the liquid-graphite interface, based on Schiff-base condensation between six dialkoxylated isophthalaldehyde ($IPA_n$) and six *p*-phenylenediamine (pP) molecules in 1,2,4-trichlorobenzene (TCB) solution. These macrocycles count 66-atoms rings of ca. 3 nm in diameter and consist of 12 imine bonds and 12 *n*-octadecyl sidechains pointing outwards. Synthesis of such structures in solution would be especially challenging (if not impossible) due to the floppiness/conformational disorder of the imine-linked phenylene backbones. We use scanning tunneling microscopy (STM) to characterize *in situ* macrocyclization with a submolecular resolution and confirm the formation of 2D arrays of monodisperse [6+6] Schiff-base macrocycles as the main product. Furthermore, by varying the length of alkoxy side chains on $IPA_n$ precursor (Scheme 1), we were able to control the surface products between macrocycles, linear oligomers or extended polymers. Molecular modeling using density functional theory (DFT) calculations explains the role of alkyl chain length as a 'knob' to tweak the molecular surface packing density. Molecular dynamics (MD) simulations reveals the role of the competitive adsorption between solvent, monomer precursors and intermediates in determining the onset of surface reactions, which promotes different products on surface.

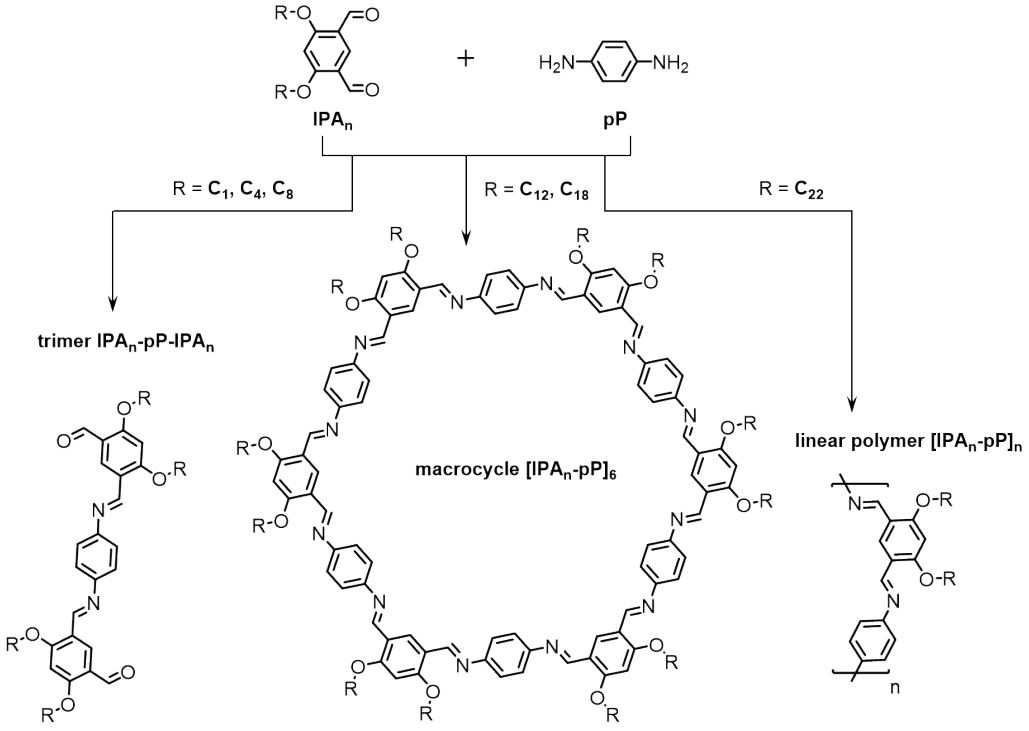


**Scheme 1.** Chemical structures of *p*-phenylenediamine (pP) and dialkoxylated isophthalaldehyde ($IPA_n$) monomers and the corresponding products at the TCB/HOPG interface.

## Results and Discussion

**On-surface [6+6] cyclization**. STM was used to image the assemblies resulting from *in situ* Schiff-base condensation between $IPA_{18}$ and pP at the liquid/HOPG interface. By drop-casting a 1:1 molar ratio mixture of $IPA_{18}$ and pP (0.1 mM each) in 1,2,4-trichlorobenzene (TCB) and octanoic acid (2.5 % v/v as an acid catalyst) onto HOPG substrate, cyclic hexagonal features emerged at the TCB/HOPG interface after 5 min (Figure 1a). The external diameter of the resolved hexagons measures 3.0 ± 0.1 nm, which is comparable to imine-linked cyclododecaphenylene macrocycles. UV-Vis absorption spectra acquired on the same reaction mixture revealed a redshifted band which is indicative of increased conjugation length, *i.e.* C=N bond formed between phenyl rings (Figure S1.1). The periodic spacing of the hexagonal unit cell (5.3 ± 0.1 nm) is defined by 12 alkyl chains that intedigitate with the ones of the neighbouring macrocycles (Figure 1a). While macrocyclic backbones are more clearly resolved at high tunneling current, this measurement requires positioning of the STM tip very close to the surface, which consequently disrupts the monolayer after repeated scans (Figure S2.1). Low-current STM imaging revealed a honeycomb structure on the surface, as depicted in Figure 1b and S2.2. Interestingly, the conversion of open-chain oligomers into macrocycles was occasionally captured at 20 Hz scanning rate and within a typical STM time frame (Figures S2.4, S2.5). The observed dynamic and reversible process at the solid-liquid interface would explain the formation of macrocycle arrays extending over hundred nanometers (Figure 1c) and can reach 500 × 500 $nm^2$ in size (Figure S2.3).

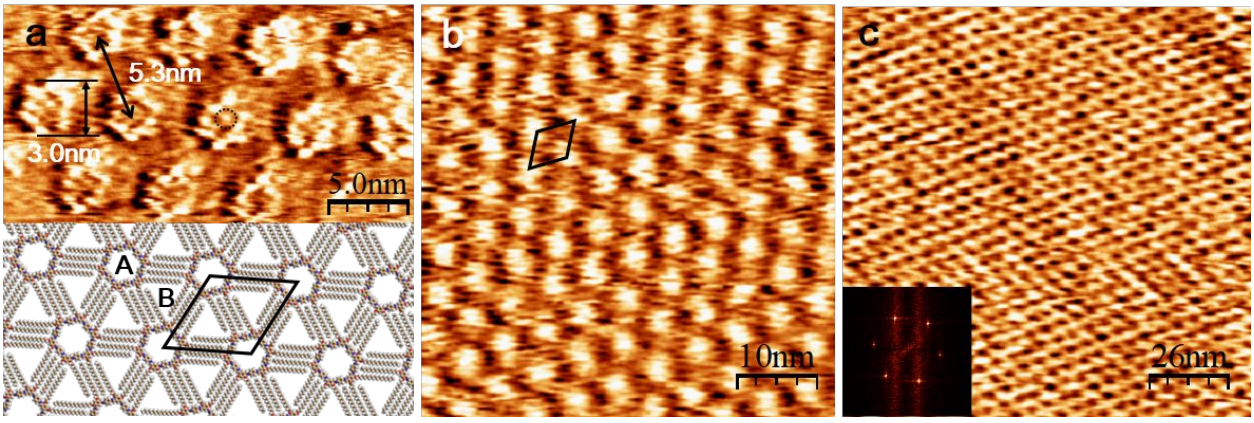


**Figure 1** STM images of $(IPA_{18}\text{-}pP)_6$ macrocycles formed at TCB/HOPG interface with monomer concentration of 0.1mM and scanned at (a) high and (b)-(c) low tunneling current. The black dotted circle on (a) indicates possible co-adsorbed TCB solvent inside the macrocycle. The inset on (c) shows the 2D-FFT of a 130×130 $nm^2$ single domain. Tunneling parameters: (a) $V_{bias}$ = 800 mV, $I_{set}$ = 160 pA; (b) (c): $V_{bias}$ = 900 mV, $I_{set}$ = 5-10 pA.

The [6+6] imine-linked macrocycle has rarely been reported in solution synthesis, as they usually suffer from low yield even recurring to supramolecular preorganization and metal templated synthesis.[41-43] Our observation of the high-yield [6+6] macrocyclization on a surface is also far from trivial, as the ditopic monomers of such symmetry usually favor open-chain polymerization. In fact, unsubstituted isophthalaldehyde reacts with pP to form exclusively linear zigzag oligomers/polymers on graphite surface.[44,45] Moreover, the gas-phase DFT calculations of this macrocycle suggests destabilization by 3.9 kcal·mol$^{-1}$ compared to the open-chain polymer due to intramolecular strain (sterically hindered hydrogens at the ring periphery, see Figure S6.2). We therefore inferred that the alkyl side-chains on the IPA monomer play a key role in driving the on-surface macrocyclization.

**Tuning the reaction with alkyl chains**. To investigate the effect of alkyl chains on the probed reaction, we surveyed the on-surface condensation between pP and *O*-alkylated IPA bearing chains of different lengths (Figure 2). Similar experimental conditions were applied except that concentrations were varied due to different solubility and graphite surface affinity of each $IPA_n$ monomer. In fact, optimizing monomer concentration is crucial for achieving monolayer formation on the surface, as high concentrations led to massive oligomer/polymer aggregates and multilayers (Figures S2.6-S2.11).

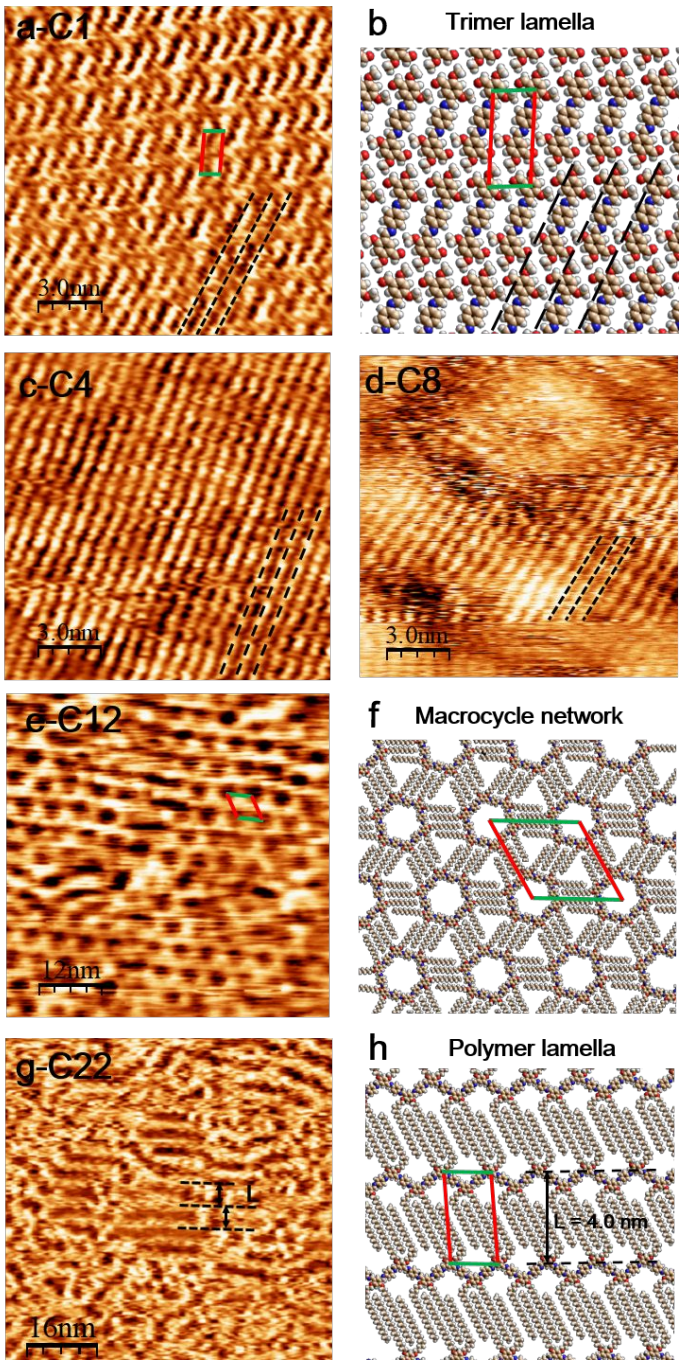


**Figure 2** Schiff bases produced by condensation pP and *O*-alkylated IPAs of increasing chain length at the TCB/HOPG interface. STM images of the close-packed (a) $IPA_1$-pP-$IPA_1$ trimers with monomer concentration of 0.25 mM, (c) $IPA_4$-pP-$IPA_4$ trimers with monomer concentration of 0.21 mM, and (d) $IPA_8$-pP-$IPA_8$ trimers with monomer concentration of 0.3 mM. (b) Molecular model of the close-packed trimers observed in (a), (c), (d), and alkyl chains are simplified to methyl groups for clarity. (e) An STM image of $(IPA_{12}\text{-pP})_6$ macrocycle assembly with monomer concentration of 0.2 mM and (f) the corresponding

molecular model. (g) STM image of $(IPA_{22}\text{-}pP)_n$ polymers with monomer concentration of 0.05 mM and (h) the corresponding molecular model of the polymers in ordered regions. Tunneling parameters: (a), (c), (d) $V_{bias}$ = 800 mV, $I_{set}$ = 120 pA; (e) $V_{bias}$ = 900 mV, $I_{set}$ = 5-10 pA; (g) $V_{bias}$ = 900 mV, $I_{set}$ = 200 pA.

The STM shows that IPA bearing short alkyl chains (*i.e.* $C_1$, $C_4$ and $C_8$) forms exclusively close-packed lamellar structures at the TCB/HOPG interface (Figures 2a, c, d). The linear submolecular feature of the lamellae is inconsistent with the zigzag profile of the 1D-polymer backbones, but compatible with a tiling of close-packed trimers condensed from 2 $IPA_1$ and 1 pP monomers (see dotted lines in Figures 2a-d). The molecular model of the proposed structure optimized by molecular mechanics yields unit cell with a = 0.9 nm, b = 2.1 nm and α = 86°, in agreement with those obtained from STM measurement (a = 0.9 ± 0.1 nm, b = 2.0 ± 0.1 nm and α = 86 ± 1°). The lamellar spacing remains the same in the case of $IPA_1$, $IPA_4$ and $IPA_8$ (Table 1 and Figures 2a, c, d) which suggests that these short alkyl chains stick out from the (substrate) surface and, hence, do not affect the geometry of the lamellar network. The formation of 2D structures with alkyl groups detached from surface may occur to facilitate close-packing of the attached (hetero)aromatic cores on graphite surface.[46-48]

The reaction of $IPA_{12}$ with pP leads to the formation of a honeycomb network ($a = b$ = 4.6 nm and α = 120°) similar to that of the $IPA_{18}$ previously discussed, suggesting formation of $(IPA_{12}\text{-}pP)_6$ macrocycle arrays at the TCB/HOPG interface (Figures 2e, 2f). However, a further elongation of IPA alkyl chains from $C_{18}$ to $C_{22}$ produces upon reaction open-chain polymers (Figure 2g). Their appearance is characterized by linear features connected by curves, similar to those reported for other 'rigid-rod' conjugated polymers that possess long alkyl chains. Those curved regions are a fingerprint of folded polymer backbones, stabilized *via* intramolecular alkyl chains interdigitation.[49-51] The interlamellar spacing of the locally ordered regions is measured as L = 4.0 ± 0.2 nm, a value that implies a partial interdigitation of tilted docosyl ($C_{22}$) chain of the neighboring lamellae (3.0 nm × cos 30° = 2.6 nm), since the width of the zigzag polymer backbones is approximately 1.4 nm (Figure 2h). Although the polymer terminals cannot be precisely defined on the STM image, the locally ordered regions can only be attributed to the self-assembly of the covalently linked polymer strands. Based on the statistic length distribution of the straight lines (6 – 18 nm) in those regions, it can be inferred that phenylene-*bis*-imine chains of 5-16 repeat units have formed on HOPG.

**Table 1.** Summary of on-surface Schiff-base formation from $IPA_n$ and pP monomers and unit cell parameters of the corresponding supramolecular structures.

| Oligomer/ Polymer | R-chain | Network | Plane group | Unit Cell (UC) | | | Area | Packing Density |
|---|---|---|---|---|---|---|---|---|
| | | | | a/nm | b/nm | α/deg | $nm^2$/UC | n($IPA_n$), n(pP)/$nm^2$ |
| $IPA_n$-pP-$IPA_n$ trimer | $C_1$ | lamella | *P*2 | 0.9 ± 0.1 | 2.0 ± 0.1 | 86 ± 1 | 1.8 | 1.1, 0.56 |
| | $C_4$ | lamella | *P*2 | 0.9 ± 0.1 | 2.1 ± 0.1 | 86 ± 1 | 1.8 | 1.1, 0.56 |
| | $C_8$ | lamella | *P*2 | 0.9 ± 0.1 | 2.1 ± 0.1 | 86 ± 1 | 1.8 | 1.1, 0.56 |
| $(IPA_n\text{-pP})_6$ macrocycle | $C_{12}$ | macrocycle network | *P*6 | 4.6 ± 0.1 | 4.6 ± 0.1 | 120 | 18.3 | 0.49, 0.49 |
| | $C_{18}$ | macrocycle network | *P*6 | 5.3 ± 0.1 | 5.3 ± 0.1 | 120 | 24.3 | 0.37, 0.37 |
| $[IPA_{22}\text{-pP}]_n$ polymer[a] | $C_{22}$ | lamella | *P*2 | 2.2 | 4.1 | 88 | 9.0 | 0.22, 0.22 |

[a.]The unit cell was deduced from molecular modeling, assuming extended polymer backbones.

**Insights into surface product formation and self-assembly**. The substitution of isophthalaldehyde groups with alkyl chains of various lengths led to various products and supramolecular assemblies on surface (Figure 2). The energy balance between macrocycles, open-chain oligomers and polymers can be evaluated from the molecular strain induced by the surface confinement and optimal 2D-supramolecular packing upon varying the alkyl chain length. To investigate the feasibility of different oligomer/polymer chain conformations and the corresponding supramolecular structures, molecular mechanics and DFT cluster calculations were performed on all observed supramolecular systems by considering the full range of alkyl chain lengths ($C_1$-$C_{22,}$ Figure 3).

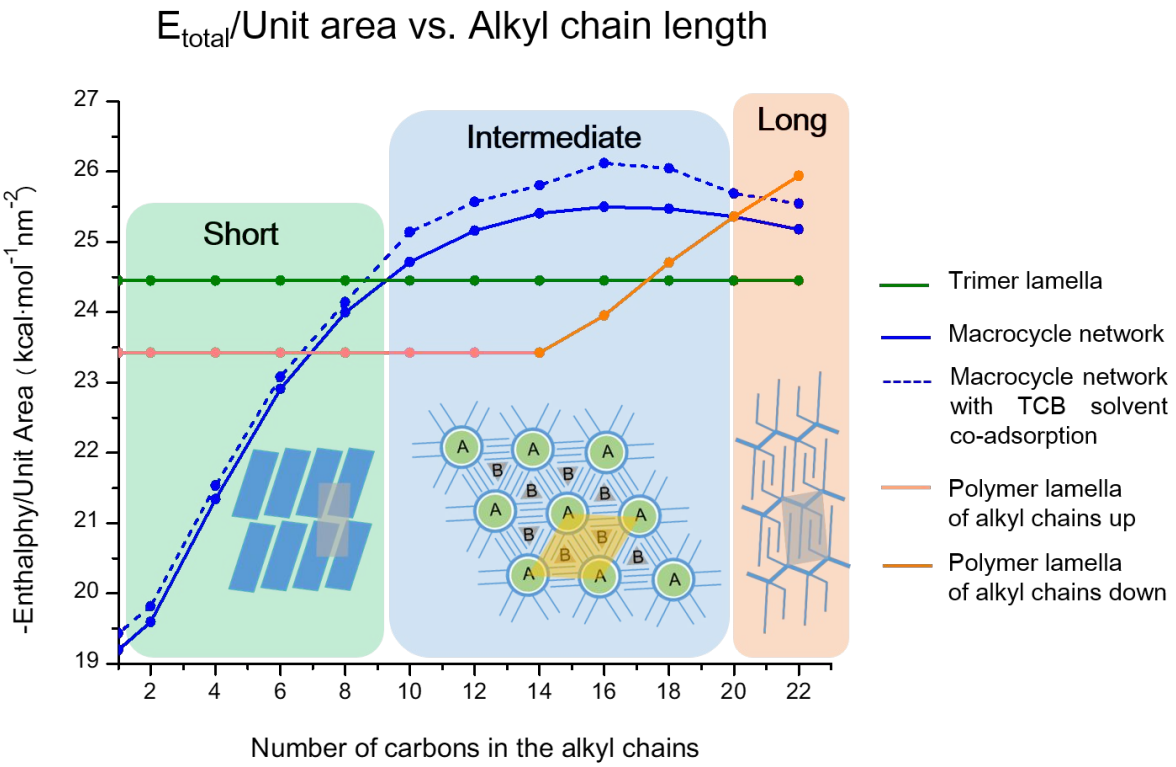


**Figure 3**. Packing enthalpy as a function of IPA alkyl-chain length, showing the progressive transition through three alkyl chain regimes.

Molecular mechanics modelling of two-dimensional clusters in gas phase suggests that short chains (from $C_1$ to $C_8$) are not sufficient to stabilize the periodic open-pore macrocyclic tiling. Instead, both trimers and zigzag polymers achieve a denser packing since in both structures lateral alkyl chains are desorbed from the surface, and, consequently, the packing enthalpy is independent from the chain length (see molecular models in Figure 2). The calculated packing density (number of atoms per unit area) indicates that the trimers have the tendency to pack more tightly than zigzag polymers (Figure S7.1). The alkyl chains tethered at each kink of the polymers' zigzag disrupt the efficient packing. In contrast, with alkyl chains at the two IPA-terminals, trimers adopt a $C_2$ symmetry that allows close packing on surface (Figure 2b). The unreacted aldehyde groups on the trimers should disfavor this product with respect to infinite polymer by 9.6 kcal/mol · per unit cell, *i.e.* the enthalpy gain of imine bond formation derived from the experimental values of bond dissociation energies at room temperature.[52] Such loss of formation enthalpy could be largely compensated by van der Waals interaction between the close-packed aromatic backbones (4.9 kcal/mol · per unit cell) and higher surface adsorption energy than that of zigzag polymers (8.5 kcal/mol · per unit cell), hence resulting in the exclusive formation of trimers on surface in the short alkyl chain regime.

When extending the alkyl chains from $C_{10}$ to $C_{18}$, the enthalpy balance is tipped towards macrocycle assembly, in which the alkyl chains interactions and adsorption energy continue to increase and thus effectively stabilize the porous network on surface (blue line, Figure 3). On the other hand, for the hexadecyl and longer alkyl chains, zigzag polymers with interdigitated alkyl chains adsorbed on the surface (dark orange line) become stable enough to overwhelm the polymer packing of alkyl chains projecting from the surface (light orange line) and the close-packed trimers (green line, Figure 3). However, the proposed polymer lamellae are still insufficient to compete with the macrocycle networks. In order to interdigitate efficiently, half of the alkyl chains at the kinks of the zigzag polymers must bend through four methylene units in eclipsed conformation (Figure 2h). The intramolecular strain due to the alkyl chain bending ($2 \times 5.2$ kcal/mol · per unit cell, as ascertained by DFT calculations[53]) is much higher than that released from converting the macrocycles to open-chain polymers (1.3 kcal/mol · per unit cell). Therefore, in the intermediate alkyl chain regime (blue shaded area in Figure 3), the macrocycle arrays with alkyl chains fully extended are dominant on surface.

Further extending the alkyl chains from $C_{20}$ to $C_{22}$ leads to the open pores B larger than the macrocyclic pores A in the arrays (Figure S7.2), which eventually decreases the adsorption energy density, and thus destabilizes the macrocycle structures with respect to the zigzag polymer lamellae. Overall, each of the three experimentally observed supramolecular systems predominates in certain regime of the chain length "phase diagram" (Figure 3), and the most stable product predicted by calculations is consistent with experimental observations (Figures 1, 2). The entropy loss of the above-mentioned molecular aggregates on surface has not been discussed so far. The Schiff bases of similar structurally flexible polyimine backbones could be thought of featuring comparable conformational entropy loss when confined on surface, except for trimers that would have an additional entropy contribution from the alkyl chains desorbed from the surface. The translational entropy, on the contrary, would favor formation of large species like macrocycles and polymers, as they take more space on the surface thus allowing small species to leave the surface and return in solution. However, to accurately estimate entropy of this reactive, multicomponent and structurally flexible/large molecular system, as compared to the current studies,[54,55] is still at an early stage and thus is beyond the scope of our work.

Furthermore, the planar aromatic solvent molecule, TCB, has been observed to co-adsorb in cyclic supramolecular clusters and hence to stabilize porous polymorphic structures on surface.[56] Likewise, a small dotted feature, indicated with a circled bright spot, could be seen in Figure 1a. Modeling of TCB co-adsorption inside the macrocycle cavities (pores A and/or B) shows a slight increase (0.2 - 0.6 kcal/mol/nm$^2$, see Table S8.1) in stabilization energy (blue dotted line in Figure 3), which does not alter the overall trend

of the relative stability of the supramolecular systems (see Supporting Information section 8 for detailed calculations).

**Role of the solvent on graphite surface**. So far, we discussed the relative stability of the different packing motifs observed on HOPG without considering the interference of solvent on surface product formation. To unravel the solvent role in selecting particular reactive species on graphite surface, classical MD simulations were applied to investigate the adsorption free energy of reaction precursors in both vacuum and TCB (Figure 4a), the details of which are provided in the Experimental Methods and Supporting Information section 9.

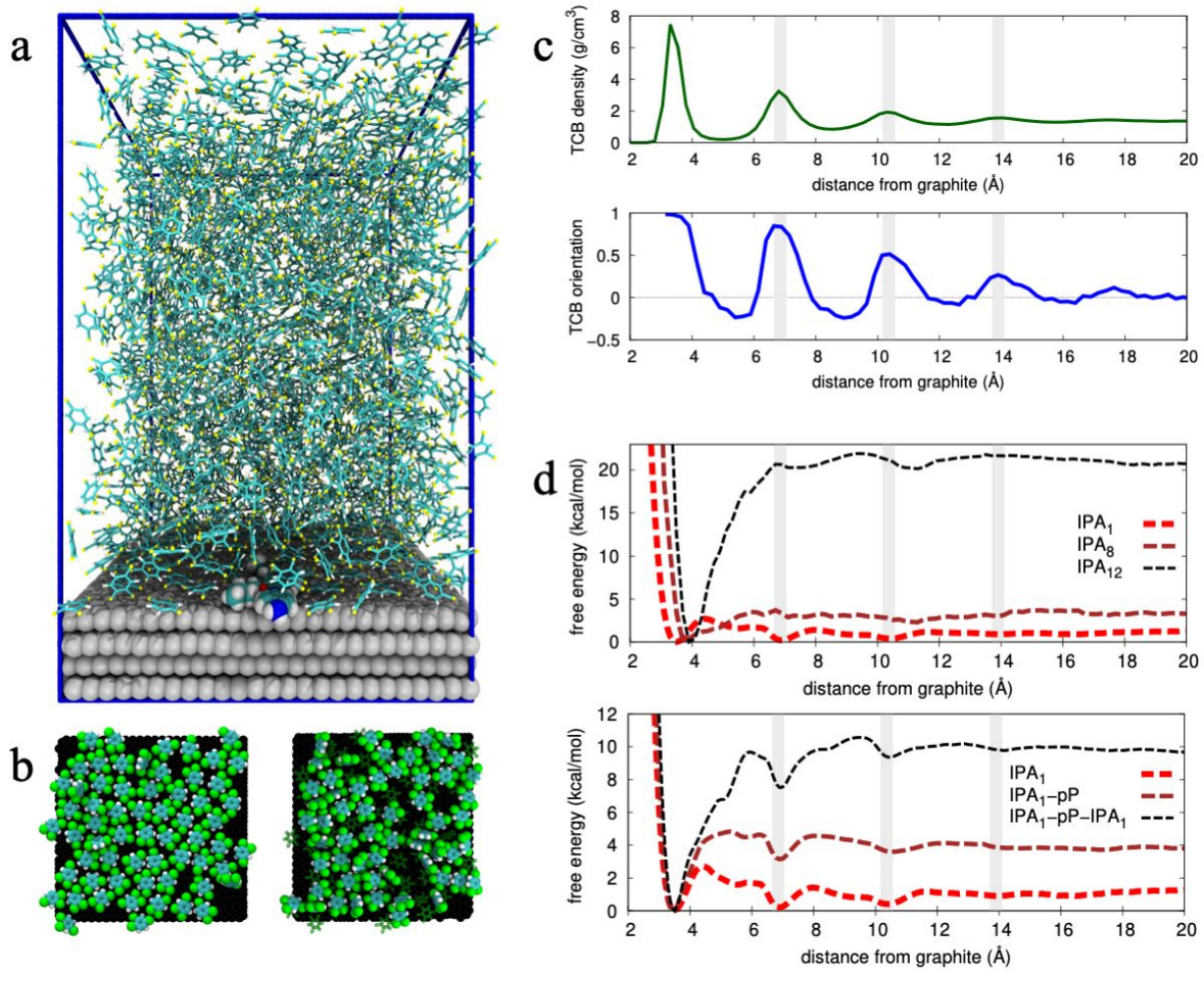


**Figure 4**. MD simulations of the target molecule at the interface with graphite. (a) Snapshot of the (60 × 60 ×102 Å$^3$) simulation box containing 1500 TCB solvent molecules and a single IPA$_4$-pP dimer adsorbed on the slab of 4 graphene layers with periodic boundary conditions. Atom color coding: carbon (gray), nitrogen

(blue), oxygen (red), hydrogen (white), chlorine (yellow). (b) Snapshots of a cross-section of the simulated sample showing the TCB molecules composing the first (left, graphite depicted in black) and second (right, with first layer molecules shaded) adsorbed layers on graphite surface. (c) The TCB density profile along the direction normal to the surface shows three strongly structured layers at distances between 2 and 12 Å (top). The local average orientational order parameter $S$ of TCB molecules quantifies the alignment of molecular aromatic planes within the layers with respect to the surface (bottom). (d) Free energy profiles in TCB as a function of the distance between the center of mass of target molecules and the atoms of a graphite sheet, showing the effect of increasing IPA chain length (top) and oligomer size (bottom).

To provide insights into adsorption free energies in TCB, and also in light of recent experimental findings on structured solvent layers at solid-liquid (water) interfaces,[57,58] we performed a detailed investigation of the organization of TCB molecules in proximity of the graphite surface. TCB molecules were found to form organized solvation structures on the solid surface, unambiguously identified by the density peaks centered at 3.3, 6.8 and 10.3 Å from the graphite surface (Figure 4b, 4c). Meanwhile, their liquid like nature is maintained as the measured retention time of TCB molecules is longer near the surface but still compatible with a liquid phase (see Figure S9.1 for details and MD simulations movies showing the diffusion of solvent molecules). The existence of structured yet mobile solvation layers is consistent with that of MD simulated methanol in a water mixture on graphite.[57] Furthermore, the solvation layers not only possess positional order, but also adopts preferential molecular orientation with respect to the surface, measured through the local average of the orientational order parameter[59]:

$$S = \left\langle \frac{3}{2}\cos^2\left(n \cdot u_i\right) \right\rangle_i$$

, where $n$ is the normal to the graphite surface, $u_i$ is the normal to the TCB molecular plane for molecule $i$, and the angular brackets indicate an ensemble average over all molecules populating a certain distance value from the surface. The oscillations of $S$ profile are shown strictly correlated with density variation, and that the amplitude decreases with increasing the distance from the surface, as presented in the bottom panel of Figure 4c. In particular, $S$ assumes high positive values corresponding to the density maxima, revealing parallel alignment of TCB molecules to graphite, also captured as the snapshots in Figure 4b. The order parameter approaches zero at about 15 Å from the surface, indicating that an isotropic distribution of molecular orientations is achieved when moving towards the bulk of the liquid TCB phase.

We conjecture that besides the good solvent nature of TCB, the solvation layers on HOPG could interfere with the adsorption of other species, affecting the types of reactants available on the surface. When simulated in vacuum, the adsorption free energies of all target molecules are all large (10-60 kcal/mol, Figure S9.2) and proportional to the size of either molecular backbones or alkyl side chains. On the contrary, in the

presence of TCB, one main reactant, pP, does not show any affinity for the graphite surface (Figure S9.3), and short chain $IPA_n$ reactants (n ~ 1─8) exhibit negligible or rather small adsorption energies as compared to that of TCB (Figure 4d, top panel). Moreover, the simulated free adsorption profiles would exhibit local minima at the distances corresponding to the density maxima of the 2nd and 3rd solvation layers (Figures 4d, shaded areas). Therefore, small sized reaction precursors would experience these local energy barriers (1-2 kcal/mol at 300 K) slowing down the process of their adsorption and desorption, with possible relevant consequences on the reaction kinetics and selective product formation on surface. Only when the condensation reaction proceeds to yield trimers ($IPA_n$-pP-$IPA_n$, $n \leq 8$, Figure 4d, bottom panel), these new products become significantly attracted to the surface (~10 kcal/mol of free energy gain), and are expected to reside there for relatively long times (see the calculated surface retention times in Table S9.1). Alternatively, the elongation of alkyl side chains also leads to reactive species, such as $IPA_{12}$ (Figure 4d, top) and $IPA_{18}$ (Table S9.1), increasingly stable on surface.

**Conclusions**

We successfully prepared a series of different phenylene-*bis*-imines *via in situ* Schiff-base condensation in 1,2,4-trichlorobenzene at the interface with a graphite surface. Elongation of the alkyl chains on isophthalaldehyde monomers resulted a progressive transition of on-surface products from trimers to macrocycles to linear polymers as confirmed by STM imaging. Furthermore, the mechanisms of the on-surface polycondensation can be inferred from combined DFT and MM/MD simulations as follows (Scheme 2). For $IPA_n$ with short alkyl chains ($n \leq 8$), trimers with respect to the monomers and dimers, are preferentially absorbed on graphite. They eventually form the densest-packed supramolecular structures, where the head-to-head aligned aldehyde groups are hindered from further reactions. Elongating alkyl side chains of $IPA_n$ leads to attenuation of the solvent effect. Reactive species, such as $IPA_n$ ($n > 8$), become increasingly stable on surface, and so do the pP-$IPA_n$ dimers. As pP alone has no affinity to graphite in TCB, the on-surface polycondensation is very unlikely to start with the monomers but at least the pP-$IPA_n$ dimers. Their adsorption free energies become rather large (tens of kcal/mol), enabling a high number of dimers to remain at the surface vicinity and sufficient time (surface retention time is almost infinite) to diffuse on the surface. Consequently, the self-assembly of dimers can reactively self-assemble into thermodynamically favored proto-macrocyclic networks, which, compared to randomly deposited monomers, significantly increases the chance of forming covalently linked macrocycles. Further lengthening alkyl chains (*i.e.* $C_{22}$) of $IPA_n$ results in mostly disordered open-chain polymers on graphite surface, as now the surface adsorption energy disfavors macrocycle assembly possessing large open pores, and disorder flexible polymer chains

are entropically more favored. Overall, this complex behavior is a manifestation of a delicate balance between intramolecular strain, imine bond formation, intermolecular and molecular-substrate interactions. In addition, solvent interference selectively drives specific reactants and oligomers onto the surface, promoting the reactions towards the corresponding thermodynamically stable products on surface.

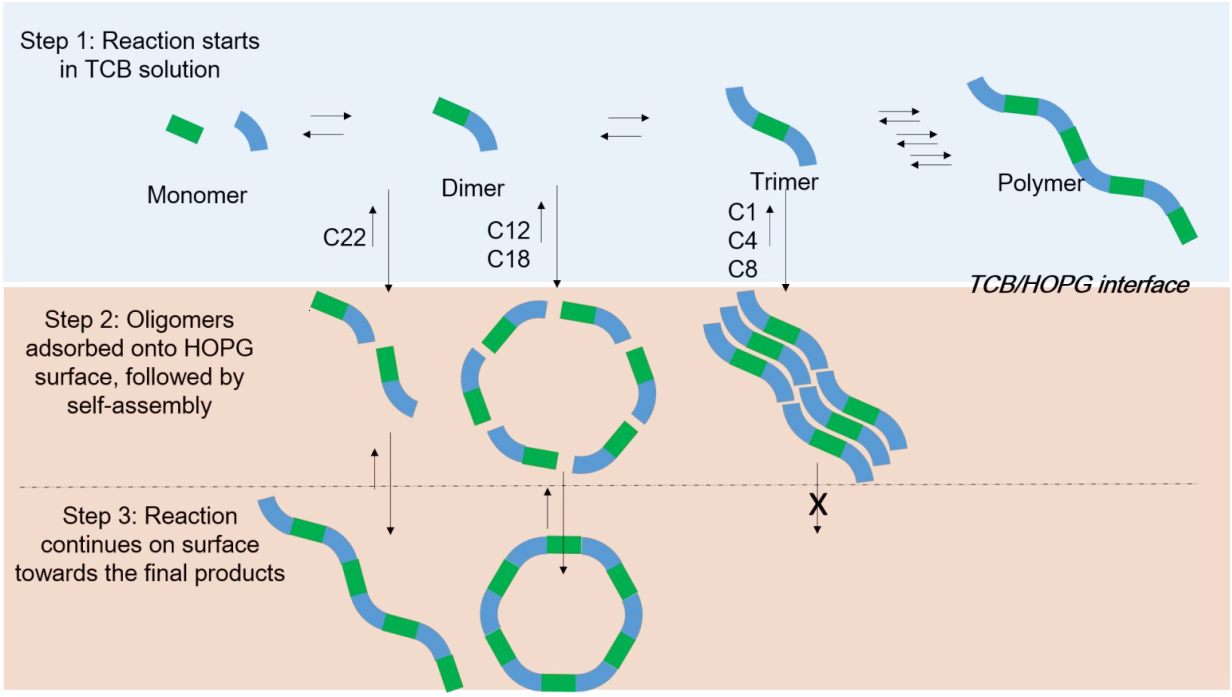


**Scheme 2.** Proposed mechanisms of on-surface polycondensation of $IPA_n$ and pP at the TCB/HOPG interface.

Our study represents the primary case of on-surface synthesized macrocycles under ambient conditions. Compared to the macrocyclization under ultra-high vacuum, our approach does not require harsh conditions (*i.e.* elevated temperature for molecular evaporation) and, as such, allows different organic precursors to be deposited in any molar ratio. The key role of the solvent must be the object of future research, as it would allow the control of on-surface DCC products *via* solvents of different properties such as polarity, aromaticity and viscosity. Furthermore, thanks to solid-liquid interface and reversible DCC bond formation, metastable products (open-chain oligomers) can be efficiently converted into macrocycles, yielding a full surface coverage of monodisperse [6+6] macrocycles. Our combined DCC and on-surface synthesis can be potentially applied to realize a variety of macrocyclic periodic patterns featuring multiple components (*i.e.* building blocks, guest molecules), pore sizes and functional groups attached to the periphery of the cavities (*i.e.* metal coordination sites), thus paving the way towards nano-patterning of multifunctional surface.

## Experimental Methods

**Materials.** *P*-phenylenediamine (pP) was purchased from Sigma-Aldrich and used without further purification. 2,4-Bis(octadecyloxy)-isophtalaldehyde ($IPA_{18}$), 2,4-Bis(dodecyloxy)-isophtalaldehyde ($IPA_{12}$), 2,4-Bis(octyloxy)-isophtalaldehyde ($IPA_8$), 2,4-Bis(butoxy)-isophtalaldehyde ($IPA_4$), 2,4-Bis(methoxy)-isophtalaldehyde ($IPA_1$) and 2,4-Bis(docosyloxy)-isophtalaldehyde ($IPA_{22}$) were synthesized according to reported procedures.[60] All synthesis details and full characterization of the desired molecules are provided in the Supporting Information section 10.

**Sample preparation.** The reaction mixture for *in situ* $IPA_{18}$ + pP macrocyclization on graphite surface was prepared by premixing $IPA_{18}$ and pP solution (0.2 mL and 1mM each in TCB; 0.1% v/v DMF was applied in pP solution to ensure its solubilisation in TCB), followed by dilution up to 2 mL total volume in TCB, and then addition of 50μL octanoic acid. To avoid the formation of oligomers/polymers in the reaction mixture and their aggregation on the surface over a period of time (>1 hour, see Figure S2.12), the freshly prepared reaction mixture was immediately drop-casted onto the HOPG for STM scanning. The same experimental procedure was repeated on the other $IPA_n$ monomers except that concentrations were adjusted to obtain a molecular monolayer coverage. More experimental data are presented in the Supporting Information section 2.

**STM characterization.** 1,2,4-Trichlorobenzene (98%) and octanoic acid (99%) were purchased from Sigma-Aldrich and used without further purification. STM experiments were carried out on a Nanoscope Multimode 8 with A-scanner and standard STM scanning head at room temperature using a mechanically cut Pt/Ir tip. All solution samples (6 μL) were applied onto the basal (0001) plane of freshly cleaved HOPG. The self-assembled molecular network (SAMN) was visualized by STM using constant current mode at the solid/liquid interface. Molecular resolution was achieved at positive tip biases with the sample grounded. Image analysis and calibration was performed using WSxM software.[61]

**Molecular modeling and DFT calculations.** All DFT calculations were carried out using the Gaussian 16 program package.[62] The macrocycle and oligomer structures were geometry optimized by B3LYP functional with the 6-31G(d) basis set, and the TCB solvent co-adsorption was calculated by M06-2X functional with the 6-31G(d) basis set. The supramolecular structures were built as molecular clusters using experimentally observed unit cell and optimized by MM+ calculations in HyperChem 8.0. More calculation details are provided in the Supporting Information sections 4-6, 8.

**Molecular Dynamics Simulations**. All simulations were performed using the NAMD software,[63] employing the GAFF force field,[64] with PBE0//cc-pVTZ atomic charges for TCB, monomers, dimers and

trimers, and a Lennard-Jones parameterization of graphite.[65] Adsorption energies were obtained from NVT simulations at 300 K of a graphite/TCB slab containing one target molecules, in which an adaptive biasing force[66] was applied to the center of mass of a reactant or product in order to explore its free energy profile as a function of the distance from the graphite surface. Full simulations details and further results are given in the Supporting Information section 9.

**Supporting Information**

Supporting Information is available free of charge *via* the Internet at http://pubs.acs.org.

Figures S1.1, S2.1-12, S3.1-2, S4.1-4, S5.1-2, S6.1-4, S7.1-2, S8.1-4, S9.1-2, Tables S8.1, S9.1, references, and movies. UV-Vis absorption spectra of reaction mixtures; additional STM images of *in situ* polymerization; molecular modeling of the self-assembly of monomers and oligomers; MM+ optimization of supramolecular structures; DFT calculations of molecular strain; additional plots of packing density and pore size *versus* alkyl chain length; combined DFT and MM+ simulations of TCB solvent co-adsorption in macrocycle networks; MD simulations of molecular adsorption at the solvent/graphite interface; synthesis of $IPA_n$ compounds and their precursors; MD simulations movies of the diffusion of solvent molecules.

**Acknowledgements**

E. O. and D. F. P. are supported by the Natural Sciences and Engineering Research Council of Canada (NSERC) through individual Discovery Grants. C.F. acknowledges the postdoctoral fellowship from the Natural Sciences and Engineering Research Council of Canada (NSERC). The work was also supported by project No.: 18-20357S (awarded by Czech Science foundation) and project No.: 21902063 (awarded by the National Natural Science Foundation of China). The authors also acknowledge the assistance provided by the Research Infrastructures NanoEnviCz (Project No. LM2015073) supported by the Ministry of Education, Youth and Sports of the Czech Republic and the project Pro-NanoEnviCz (Reg. No. CZ.02.1.01/0.0/0.0/16_013/0001821) supported by the Ministry of Education, Youth and Sports of the Czech Republic and the European Union - European Structural and Investments. Computer time for MD simulations was provided by the Pôle Modélisation HPC facilities of the Institut des Sciences Moléculaires, co-funded by the Nouvelle Aquitaine region, as well as by the MCIA (Mésocentre de Calcul Intensif Aquitain) resources of the Université de Bordeaux and of the Université de Pau et des Pays de l'Adour.

**References**

1. Pedersen, C. J. Cyclic Polyethers and Their Complexes with Metal Salts. *J. Am. Chem. Soc.* **1967**, *89*, 7017─7036.
2. Cram, D. J.; Cram, J. M. Host-Guest Chemistry. *Science* **1974**, *183*, 803─809.
3. Lehn, J.-M. Supramolecular Chemistry. Wiley VCH: Weinheim, 1995.
4. Driggers, E. M.; Hale, S. P.; Lee, J.; Terrett, N. K. The Exploration of Macrocycles for Drug Discovery — An Underexploited Structural Class. *Nat. Rev. Drug Discov.* **2008**, *7*, 608─624.
5. Marsault, E.; Peterson, M. L. Macrocycles Are Great Cycles: Applications, Opportunities, and Challenges of Synthetic Macrocycles in Drug Discovery. *J. Med. Chem.* **2011**, *54*, 1961─2004.
6. Schulze, M.; Kunz, V.; Frischmann, P. D.; Würthner, F. A Supramolecular Ruthenium Macrocycle with High Catalytic Activity for Water Oxidation That Mechanistically Mimics Photosystem II. *Nat. Chem.* **2016**, *8*, 576─583.
7. Hoekman, S.; Kitching, M. O.; Leigh, D. A.; Papmeyer, M.; Roke, D. Goldberg Active Template Synthesis of a [2]Rotaxane Ligand for Asymmetric Transition-Metal Catalysis. *J. Am. Chem. Soc.* **2015**, *137*, 7656─7659.
8. Kim, H. N.; Ren, W. X.; Kim, J. S.; Yoon, J. Fluorescent and Colorimetric Sensors for Detection of Lead, Cadmium, and Mercury Ions. *Chem. Soc. Rev.* **2012**, *41*, 3210─3244.
9. Ghale, G.; Nau, W. M. Dynamically Analyte-Responsive Macrocyclic Host–Fluorophore Systems. *Acc. Chem. Res*. **2014**, *47*, 2150─2159.
10. Iyoda, M.; Yamakawa, J.; Rahman, M. J. Conjugated Macrocycles: Concepts and Applications. *Angew. Chem. Int. Ed.* **2011**, *50*, 10522─10553.
11. Ball, M.; Zhang, B.; Zhong, Y.; Fowler, B.; Xiao, S.; Ng, F.; Steigerwald, M.; Nuckolls, C. Conjugated Macrocycles in Organic Electronics. *Acc. Chem. Res.* **2019**, *52*, 1068─1078.
12. Rodgers, S. J.; Ng, C. Y. Raymond, K. N. High-Dilution Synthesis of Macrocyclic Polycatecholates. *J. Am. Chem. Soc.* **1985**, *107*, 4094─4095.
13. Martí-Centelles, V.; Pandey, M. D.; Burguete, M. I.; Luis, S. V. Macrocyclization Reactions: The Importance of Conformational, Configurational, and Template-Induced Preorganization. *Chem. Rev.* **2015**, *115*, 8736─8834.
14. Whiteoak, C. J.; Salassa, G.; Kleij, A.W. Recent Advances with π-Conjugated Salen Systems. *Chem. Soc. Rev.* **2012**, *41*, 622─631.
15. Fan, Q.; Gottfried, M.; Zhu, J. Surface-Catalyzed C–C Covalent Coupling Strategies toward the Synthesis of Low-Dimensional Carbon-Based Nanostructures. *Acc. Chem. Res.* **2015**, *48*, 2484─2494.
16. Campbell, C. T.; Sellers, J. R. V. The Entropies of Adsorbed Molecules. *J. Am. Chem. Soc.* **2012**, *134*, 18109─18115.
17. Lafferentz, L.; Eberhardt, V.; Dri, C.; Africh, C.; Comelli, G.; Esch, F.; Hecht, S.; Grill, L. Controlling On-Surface Polymerization by Hierarchical and Substrate-Directed Growth. *Nat. Chem.* **2012**, *4*, 215─220.
18. Lin, T.; Shang, X.S.; Adisoejoso, J.; Liu, P.N.; Lin, N. Steering On-Surface Polymerization with Metal-Directed Template. *J. Am. Chem. Soc.* **2013**, *135*, 3576─3582.
19. Eichhorn, J.; Nieckarz, D.; Ochs, O.; Samanta, D.; Schmittel, M.; Szabelski, P. J.; Lackinger, M. On-Surface Ullmann Coupling: The Influence of Kinetic Reaction Parameters on the Morphology and Quality of Covalent Networks. *ACS Nano* **2014**, *8*, 7880─7889.
20. Zhang, C.; Sun, Q.; Chen, H.; Tan, Q.; Xu, W. Formation of Polyphenyl Chains through Hierarchical Reactions: Ullmann Coupling Followed by Cross-Dehydrogenative Coupling. *Chem. Commun.* **2015**, *51*, 495─498.
21. Lipton-Duffin, J. A.; Ivasenko, O.; Perepichka, D. F.; Rosei, F. Synthesis of Polyphenylene Molecular Wires by Surface-Confined Polymerization. *Small* **2009**, *5*, 592−597.

22. Fan, Q.; Wang, C.; Han, Y.; Zhu, J.; Hieringer, W.; Kuttner, J.; Hilt, G.; Gottfried, J. M. Surface-Assisted Organic Synthesis of Hyperbenzene Nanotroughs. *Angew. Chem. Int. Ed.* **2013**, *52*, 4668─4672.
23. Fan, Q.; Wang, T.; Dai, J.; Kuttner, J.; Hilt, G.; Gottfried, J. M.; Zhu, J. On-Surface Pseudo-High-Dilution Synthesis of Macrocycles: Principle and Mechanism. *ACS Nano* **2017**, *11*, 5070─5079.
24. Chen, M.; Shang, J.; Wang, Y.; Wu, K.; Kuttner, J.; Hilt, G.; Hieringer, W.; Gottfried, J. M. On-Surface Synthesis and Characterization of Honeycombene Oligophenylene Macrocycles. *ACS Nano* **2017**, *11*, 134─143.
25. Reecht, G.; Bulou, H.; Scheurer, F.; Speisser, V.; Carriere, B.; Mathevet, F.; Schull, G. Oligothiophene Nanorings As Electron Resonators for Whispering Gallery Modes. *Phys. Rev. Lett.* **2013**, *110*, 056802: 1─5.
26. Nacci, C.; Ample, F.; Bleger, D.; Hecht, S.; Joachim, C.; Grill, L. Conductance of a Single Flexible Molecular Wire Composed of Alternating Donor and Acceptor Units. *Nat. Commun.* **2015**, *6*, 7397─7404.
27. Schlütter, F.; Rossel, F.; Kivala, M.; Enkelmann, V.; Gisselbrecht, J.-P.; Ruffieux, P.; Fasel, R.; Müllen, K. π-Conjugated Heterotriangulene Macrocycles by Solution and Surface-Supported Synthesis toward Honeycomb Networks. *J. Am. Chem. Soc.* **2013**, *135*, 4550─4557.
28. Steiner, C.; Gebhardt, J.; Ammon, M.; Yang, Z.; Heidenreich, A.; Hammer, N.; Görling, A.; Kivala, M.; Maier, S. Hierarchical On-Surface Synthesis and Electronic Structure of Carbonyl-Functionalized One- and Two-Dimensional Covalent Nanoarchitectures. *Nat. Commun.* **2017**, *8*, 14765: 1─11.
29. Liu, M.; Li, S.; Zhou, J.; Zha, Z.; Pan, J.; Li, X.; Zhang, J.; Liu, Z.; Li, Y.; Qiu, X. High-Yield Formation of Graphdiyne Macrocycles through On-Surface Assembling and Coupling Reaction. *ACS Nano* **2018**, *12*, 12612─12618.
30. Di Giovannantonio, M.; Tomellini, M.; Lipton-Duffin, J.; Galeotti, G.; Ebrahimi, M.; Cossaro, A.; Verdini, A.; Kharche, N.; Meunier, V.; Vasseur, G.; Fagot-Revurat, Y.; Perepichka, D. F.; Rosei, F.; Contini, G. Mechanistic Picture and Kinetic Analysis of Surface-Confined Ullmann Polymerization. *J. Am. Chem. Soc.* **2016**, *138*, 16696─16702.
31. Gong, Z.; Yang, B.; Lin, H.; Tang, Y.; Tang, Z.; Zhang, J.; Zhang, H.; Li, Y.; Xie, Y.; Li, Q.; Chi, L. Structural Variation in Surface-Supported Synthesis by Adjusting the Stoichiometric Ratio of the Reactants. *ACS Nano* **2016**, *10*, 4228─4235.
32. Ciesielski, A.; El Garah, M.; Haar, S.; Kovaříček, P.; Lehn, J.-M.; Samorì, P. Dynamic Covalent Chemistry of Bisimines at the Solid/Liquid Interface Monitored by Scanning Tunnelling Microscopy. *Nat. Chem.* **2014**, *6*, 1017─1023.
33. Plas, J.; Waghray, D.; Adisoejoso, J.; Ivasenko, O.; Dehaen, W.; Feyter, S. D. Insights into Dynamic Covalent Chemistry at Surfaces. *Chem. Commun.* **2015**, *51*, 16338─16341.
34. Dienstmaier, J. F.; Gigler, A. M.; Goetz, A. J.; Knochel, P.; Bein, T.; Lyapin, A.; Reichlmaier, S.; Heckl, W. M.; Lackinger, M. Synthesis of Well-Ordered COF Monolayers: Surface Growth of Nanocrystalline Precursors *versus* Direct On-Surface Polycondensation. *ACS Nano* **2011**, *5*, 9737─9745.
35. Colson, J. W.; Woll, A. R.; Mukherjee, A.; Levendorf, M. P.; Spitler, E. L.; Shields, V. B.; Spencer, M. G.; Park, J.; Dichtel, W. R. Oriented 2D Covalent Organic Framework Thin Films on Single-Layer Graphene. *Science* **2011**, *332*, 228─231.
36. Tanoue, R.; Higuchi, R.; Enoki, N.; Miyasato, Y.; Uemura, S.; Kimizuka, N.; Stieg, A. Z.; Gimzewski, J. K.; Kunitake, M. Thermodynamically Controlled Self-Assembly of Covalent Nanoarchitectures in Aqueous Solution. *ACS Nano* **2011**, *5*, 3923─3929.

37. Dienstmaier, J. F.; Medina, D. D.; Dogru, M.; Knochel, P.; Bein, T.; Heckl, W. M.; Lackinger, M. Isoreticular Two-Dimensional Covalent Organic Frameworks Synthesized by On-Surface Condensation of Diboronic Acids. *ACS Nano* **2012**, *6*, 7234─7242.
38. Cui, D., MacLeod, J. M.; Ebrahimi, M.; Perepichka, D. F.; Rosei, F. Solution and Air Stable Host/Guest Architectures from a Single Layer Covalent Organic Framework. *Chem. Commun.* **2015**, *51*, 16510─16513.
39. Liu, C.; Park, E.; Jin, Y.; Liu, J.; Yu, Y.; Zhang, W.; Lei, S.; Hu, W. Surface-Confined Dynamic Covalent System Driven by Olefin Metathesis. *Angew. Chem. Int. Ed.* **2018**, *57*, 1869─1873.
40. Cao, L.; Yu, Y.; Lei, S. From 1D Ordered Linear Polymers to Discrete Macrocycles: Surface Adsorption and pH Take Control. *Chem. Commun.* **2018**, *54*, 12210─12213.
41. Hui, J. K.-H.; MacLachlan, M. J. [6 + 6] Schiff-Base Macrocycles with 12 Imines: Giant Analogues of Cyclohexane. *Chem. Commun.* **2006**, 2480─2482.
42. Gregoliński, J.; Ślepokura, K.; Paćkowski, T.; Panek, J.; Stefanowicz, P.; Lisowski, J. From 2 + 2 to 8 + 8 Condensation Products of Diamine and Dialdehyde: Giant Container-Shaped Macrocycles for Multiple Anion Binding. *J. Org. Chem.* **2016**, *81*, 5285─5294.
43. Chavez, A. D.; Evans, A. M.; Flanders, N. C.; Bisbey, R. P.; Vitaku, E.; Chen, L. X.; Dichtel, W. R. Equilibration of Imine-Linked Polymers to Hexagonal Macrocycles Driven by Self-Assembly. *Chem. Eur. J.* **2018**, *24*, 3989─3993.
44. Yu, Y.; Sun, J.; Lei, S. Surface-Confined Synthesis of One-Dimensional Schiff Base Polymers Investigated by Scanning Tunneling Microscopy. *J. Phys. Chem. C* **2015**, *119*, 16777─16784.
45. Liu, X.-H.; Guan, C.-Z.; Zheng, Q.-N.; Wang, D.; Wan, L.-J. Molecular Engineering of Schiff-Base Linked Covalent Polymers with Diverse Topologies by Gas-Solid Interface Reaction. *J. Chem. Phys* **2015**, *142*, 101905: 1─5.
46. Lei, S. B.; Tahara, K.; De Schryver, F. C.; Van der Auweraer, M.; Tobe, Y.; De Feyter, S. One Building Block, Two Different Supramolecular Surface-Confined Patterns: Concentration in Control at the Solid-Liquid Interface. *Angew. Chem., Int. Ed.* **2008**, *47*, 2964─2968.
47. Marie, C.; Silly, F.; Tortech, L.; Müllen, K.; Fichou, D. Tuning the Packing Density of 2D Supramolecular Self-Assemblies at the Solid−Liquid Interface Using Variable Temperature. *ACS Nano* **2010**, *4*, 1288─1292.
48. Fu, C.; Lin, H.-P.; Macleod, J. M.; Krayev, A.; Rosei, F.; Perepichka, D. F. Unravelling the Self-Assembly of Hydrogen Bonded NDI Semiconductors in 2D and 3D. *Chem. Mater.* **2016**, *28*, 951─961.
49. Mena-Osteritz, E.; Meyer, A.; Langeveld-Voss, B. M. W.; Janssen, R. A. J.; Meijer, E. W.; Bäuerle, P. Two-Dimensional Crystals of Poly(3-Alkyl-Thiophene)s: Direct Visualization of Polymer Folds in Submolecular Resolution. *Angew. Chem. Int. Ed.* **2000**, *39*, 2680─2684.
50. Keg, P.; Lohani, A.; Fichou, D.; Lam, Y. M.; Wu, Y.; Ong, B. S.; Mhaisalkar, S. G. Direct Observation of Alkyl Chain Interdigitation in Conjugated Polyquarterthiophene Self-Organized on Graphite Surfaces. *Macromol. Rapid Commun.* **2008**, *29*, 1197─1202.
51. McKeown, G. R.; Fang, Y.; Obhi, N. K.; Manion, J. G.; Perepichka, D. F.; Seferos, D. S. Synthesis of Macrocyclic Poly(3-Hexylthiophene) and Poly(3-Heptylselenophene) by Alkyne Homocoupling. *ACS Macro Lett.* **2016**, *5*, 1075─1079.
52. Luo, Y.-R. Comprehensive Handbook of Chemical Bond Energies. CRC Press: Boca Raton, 2007.
53. Murcko, M. A.; Castejon, H.; Wiberg, K. B. Carbon−Carbon Rotational Barriers in Butane, 1-Butene, and 1, 3-Butadiene. *J. Phys. Chem.* **1996**, *100*, 16162─16168.
54. Tahara, K.; Nakayama, R.; Maeda, M.; De Feyter, S.; Tobe, Y. Alkoxy Chain Number Effect on Self-Assembly of a Trigonal Molecule at the Liquid/Solid Interface. *J. Phys. Chem. C* **2019**, *123*, 27020─27029.

55. Haar, S.; Bruna, M.; Lian, J. X.; Tomarchio, F.; Olivier, Y.; Mazzaro, R.; Morandi, V.; Moran, J.; Ferrari, A. C.; Beljonne, D.; Ciesielski, A.; Samorì, P. Liquid-Phase Exfoliation of Graphite into Single- and Few-Layer Graphene with A-Functionalized Alkanes. *J. Phys. Chem. Lett.* **2016**, *7*, 2714─2721.
56. Tahara, K.; Okuhata, S.; Adisoejoso, J.; Lei, S.; Fujita, T.; De Feyter, S.; Tobe, Y. 2D Networks of Rhombic-Shaped Fused Dehydrobenzo[12]Annulenes: Structural Variations under Concentration Control. *J. Am. Chem. Soc.* **2009**, *131*, 17583─17590.
57. Voïtchovsky, K.; Giofrè, D.; Segura, J. J.; Stellacci, F.; Ceriotti, M. Thermally-Nucleated Self-Assembly of Water and Alcohol into Stable Structures at Hydrophobic Interfaces. *Nat. Commun.* **2016**, *7*, 13064: 1─9.
58. Fukuma, T.; Garcia, R. Atomic- and Molecular-Resolution Mapping of Solid–Liquid Interfaces by 3D Atomic Force Microscopy. *ACS Nano* **2018**, *12*, 11785─11797.
59. Roscioni, O. M.; Muccioli, L.; Zannoni, C. Predicting the Conditions for Homeotropic Anchoring of Liquid Crystals at a Soft Surface. 4-n-Pentyl-4′-Cyanobiphenyl on Alkylsilane Self-Assembled Monolayers. *ACS Appl. Mater. Interfaces* **2017**, *9*, 11993─12002.
60. Mezour, M. A.; Perepichka, I. I.; Zhu, J.; Lennox, R. B.; Perepichka, D. F. Directing the Assembly of Gold Nanoparticles with Two-Dimensional Molecular Networks. *ACS Nano* **2014**, *8*, 2214─2222.
61. Horcas, I.; Fernandez, R.; Gomez-Rodriguez, J. M.; Colchero, J.; Gomez-Herrero, J.; Baro, A. M. WSXM: A Software for Scanning Probe Microscopy and a Tool for Nanotechnology. *Rev. Sci. Instrum.* **2007**, *78*, 013705: 1─8.
62. Frisch, M. J.; Trucks, G. W.; Schlegel, H. B.; Scuseria, G. E.; Robb, M. A.; Cheeseman, J. R.; Scalmani, G.; Barone, V.; Mennucci, B.; Petersson, G. A.; Nakatsuji, H.; Caricato, M.; Li, X.; Hratchian, H. P.; Izmaylov, A. F.; Bloino, J.; Zheng, G.; Sonnenberg, J. L.; Hada, M.; Ehara, M.; *et al.* Gaussian 09, Revision E.01; Gaussian, Inc.: Wallingford CT, 2009.
63. Phillips, J. C.; Braun, R.; Wang, W.; Gumbart, J.; Tajkhorshid, E.; Villa, E.; Chipot, C.; Skeel, R. D.; Kalé, L.; Schulten, K. Scalable Molecular Dynamics with NAMD. *J Comput Chem* **2005**, *26*, 1781─1802.
64. Wang, J.; Wolf, R. M.; Caldwell, J. W.; Kollman, P. A.; Case, D. A. Development and Testing of a General Amber Force Field. *J Comput Chem* **2004**, *25*, 1157─1174.
65. Lu, J. P.; Li, X.; Martin R. M. Ground State and Phase Transitions in Solid $C_{60}$. *Phys. Rev. Lett.* **1992**, *68*, 1551─1554.
66. Comer, J.; Gumbart, J. C.; Hénin, J.; Lelièvre, T.; Pohorille, A.; Chipot C. The Adaptive Biasing Force Method: Everything You Always Wanted to Know but Were Afraid to Ask. *J. Phys. Chem. B* **2015**, *119*, 1129─1151.